Graphene quantum dots prevent α-synucleinopathy in Parkinson's disease

Donghoon Kim[1,2,12], **Je Min Yoo**[3,12], **Heehong Hwang**[1,4], **Junghee Lee**[5], **Su Hyun Lee**[1,2], **Seung Pil Yun**[1,2,6], **Myung Jin Park**[3], **MinJun Lee**[3], **Seulah Choi**[1], **Sang Ho Kwon**[1], **Saebom Lee**[1,2], **Seung-Hwan Kwon**[1,2], **Sangjune Kim**[1,2], **Yong Joo Park**[7], **Misaki Kinoshita**[8], **Young-Ho Lee**[8], **Seokmin Shin**[3], **Seung R. Paik**[9], **Sung Joong Lee**[4], **Seulki Lee**[7,10], **Byung Hee Hong**[3,5], and **Han Seok Ko**[1,2,6,11]

[1]Neuroregeneration and Stem Cell Programs, Institute for Cell Engineering, The Johns Hopkins University School of Medicine, Baltimore, MD, USA.

[2]Department of Neurology, The Johns Hopkins University School of Medicine, Baltimore, MD, USA.

[3]Department of Chemistry, College of Natural Science, Seoul National University, Seoul, Republic of Korea.

[4]Department of Neuroscience and Physiology, Interdisciplinary Program in Neuroscience, Dental Research Institute, School of Dentistry, Seoul National University, Seoul, Republic of Korea.

[5]Inter-University Semiconductor Research Centre, Seoul National University, Seoul, Republic of Korea.

[6]Adrienne Helis Malvin Medical Research Foundation, New Orleans, LA, USA.

[7]The Russell H. Morgan Department of Radiology and Radiological Sciences, Johns Hopkins University School of Medicine, Baltimore, MD, USA.

[8]Institute for Protein Research, Osaka University, Yamadaoka, Osaka, Japan.

[9]School of Chemical and Biological Engineering, College of Engineering, Seoul National University, Seoul, Republic of Korea.

[10]The Centre for Nanomedicine at the Wilmer Eye Institute, Johns Hopkins University School of Medicine, Baltimore, MD, USA.

[11]Diana Helis Henry Medical Research Foundation, New Orleans, LA, USA.

[12]These authors contributed equally: Donghoon Kim, Je Min Yoo.

Abstract

Though emerging evidence indicates that the pathogenesis of Parkinson's disease is strongly correlated to the accumulation[1,2] and transmission[3,4] of α-synuclein (α-syn) aggregates in the midbrain, no anti-aggregation agents have been successful at treating the disease in the clinic. Here, we show that graphene quantum dots (GQDs) inhibit fibrillization of α-syn and interact directly with mature fibrils, triggering their dis-aggregation. Moreover, GQDs can rescue neuronal death and synaptic loss, reduce Lewy body and Lewy neurite formation, ameliorate mitochondrial dysfunctions, and prevent neuron-to-neuron transmission of α-syn pathology provoked by α-syn preformed fibrils[5,6]. We observe, in vivo, that GQDs penetrate the blood-brain barrier and protect against dopamine neuron loss induced by α-syn preformed fibrils, Lewy body/Lewy neurite pathology and behavioural deficits.

Following the synthesis and analysis of graphene quantum dots (GQDs) (Supplementary Fig. 2a–c,e), we investigated the potential role of these in inhibiting α-synuclein (α-syn) fibrillization and disaggregating fibrils (Fig. 1a). In the absence of GQDs, α-syn monomers assembled into mature fibrils, as assessed by thioflavin T (ThT) fluorescence (Fig. 1b), turbidity assays (Fig. 1c) and transmission electron microscopy (TEM) analysis (Fig. 1d). The same assessments showed that the GQDs predominantly inhibited α-syn fibrillization. Moreover, GQDs induced the dissociation of α-syn fibrils into short fragments (Fig. 1e–i and Supplementary Fig. 3a), with the average length of the fragments shortening from 1 μm to 235 nm and 70 nm after 6 and 24 h, respectively (Fig. 1g,i). The average number of the shortened fragments increased during the first 24 h of incubation, suggesting that the fibrils had dissociated from the inner parts of the α-syn fibrils (Fig. 1h). However, the number of fragments started to decrease at day 3 and they were no longer detectable at day 7, indicating complete dissociation of fibrils over the course of time (Fig. 1i). Time-dependent atomic force microscopy (AFM) images show the same dissociation process, where GQDs and fibrils can be differentiated by their distinguishing height profiles (Supplementary Fig. 3b). Dot-blot assay and blue native polyacrylamide gel electrophoresis (BN–PAGE) analysis also revealed that incubation with GQDs results in the gradual reduction of fibrils in a time-dependent manner (Fig. 1j,k). Similar effects of GQDs were also observed on sonicated α-syn preformed fibrils (PFFs), which produced a higher population of monomers as the incubation period progressed (Supplementary Fig. 4a–c).

To visualize the interaction between GQDs and α-syn fibrils, GQDs were functionalized with PEGylated biotin (Supplementary Fig. 2d–g). Using streptavidin-tagged ultra-small gold particles and TEM, direct binding between GQDs and α-syn fibrils was visualized (Fig. 2a,b). Two-dimensional ^1H–^{15}N heteronuclear single-quantum coherence correlation (HSQC) NMR spectroscopy was utilized to further analyse the interaction site of ^{15}N-labelled α-syn[7,8] for GQDs and their molecular interactions at the residue level in solution.

Co-incubation with GQDs led to many residues with large chemical shifts while others had entirely disappeared (Supplementary Fig. 5). The residues that disappeared were centred on the N-terminal region, implying that the initial binding between GQDs and α-syn is largely driven by the charge interaction between the negatively charged carboxyl groups of the GQDs (Supplementary Fig. 2e) and the positively charged region of α-syn (Fig. 2c).

To better understand and elucidate the mechanism of α-syn fibril dissociation by GQDs, a 200 ns molecular dynamics (MD) simulation was performed. The structure of the α-syn fibril was adopted from the recently reported ssNMR (solid-state nuclear magnetic resonance) structure of pathologic human α-syn[9]. To facilitate the simulation process, only the non-amyloid-β component (NAC) domain (residues 71 to 82) was taken, as it is essential for α-syn fibrillization[10]. Following instantaneous binding between the GQDs and the N-terminal cross-β part of α-syn at 1 ns, the β-sheet structure of the outer monomer was completely destroyed after 50 ns; its C-terminal part was released from the core and interacted with the opposite plane of the GQDs (Fig. 2d). The time-dependent secondary structure plot, calculated by the dictionary of secondary structure of proteins (DSSP) algorithm, also shows a decrease in the β-sheet component of the outer monomer from 50 ns onwards, indicating critical structural disruption in the fibril (Fig. 2f). For further analysis, changes in the root-mean-square deviation (r.m.s.d.) of atomic positions, solvent accessible surface area (SASA) and the interaction energies of the fibril were plotted against time (Fig. 2e). Though massive changes in the r.m.s.d. and SASA values are observed after 50 ns, the changes in the total potential energy (U_{tot}) show a slight, yet continuous decline. It is confirmed that the major stabilizing/dissociation force is attributed to strong hydrophobic interactions, as changes in the van der Waals energy (E_{van}) show a decline and the electrostatic energy (E_{elec}) remains steady. The results are consistent with the 65 ns snapshot, which shows strong hydrophobic interactions between the GQDs' basal plane and valine residues (Fig. 2d). To further analyse the changes in the secondary structure of α-syn fibrils, circular dichroism (CD) spectra were obtained and the fractional secondary structures were analysed using the algorithm CONTIN/LL[11,12] (Fig. 2g,h). After 7 days, changes in the secondary structure were observed, with the β-sheet component decreasing from 53.3 ± 3.5% to 29.8 ± 3.4% and the α-helix/random coil components increasing from 4.2 ± 1.2% to 19.8 ± 1.5% and 20.1 ± 5.7% to 24.6 ± 3.6%, respectively. Collectively, the interaction between GQDs and α-syn is initiated by the charge interactions, and fibril dissociation is driven chiefly by hydrophobic interactions, accompanied by structural changes.

Based on these results, the potential role of GQDs in preventing α-syn PFF-induced pathology was explored in primary neurons. α-Syn PFF treatment leads to critical cell death, as assessed by various cell viability assays including terminal deoxynucleotidyl transferase dUTP nick end labelling (TUNEL) (Fig.3aand Supplementary Fig. 6a), alamarBlue (Fig. 3b), lactate dehydrogenase (LDH) (Fig. 3c) and neurite outgrowth assays (Supplementary Fig. 6b–d). In contrast, the presence of GQDs reduces α-syn PFF-induced cell toxicity in the same assessments. In addition, treatment of α-syn PFFs leads to a reduction in synaptic proteins such as SNAP25 and VAMP2, suggesting severe dysfunction in neuronal networks[5]. Importantly, GQDs restore the reduced synaptic protein levels provoked by α-syn PFFs (Supplementary Fig. 6e–g). Mitochondrial dysfunction is another major pathological hallmark during the progression of Parkinson's disease[13]. The effect of GQDs

on mitochondrial dysfunction and subsequent cellular respiration was thus investigated by performing oxidative stress marker 8-hydroxyguanosine (8-OHG) staining, mitochondrial complex I activity assay, MitoTracker staining, TEM analysis and seahorse assay (Supplementary Fig. 7). The treatment of α-syn PFFs causes mitochondrial damage characterized by shrinkage, decreased oxygen consumption rate and elevated reactive oxygen species (ROS) levels in neurons, but the addition of GQDs ameliorates these adverse effects.

The role of GQDs on α-syn PFF-induced Lewy body (LB)/Lewy neurite (LN)-like pathology was then evaluated. After 7 days of α-syn PFF treatment, accumulation of α-syn in the SDS-insoluble fraction was analysed by western blot, showing decreased phosphorylated α-syn (p-α-syn) accumulation with GQDs (Fig. 3d,e). In addition, p-α-syn immunoreactivity is increased in primary neurons by α-syn PFFs, whereas it is barely detectable in primary neurons treated with GQDs as assessed by α-syn phosphoserine 129 immunostaining (Fig. 3f,g). To investigate the effect of treatment time on α-syn pathology, GQDs were treated simultaneously with and 3 days pre/post α-syn PFF additions. Though the toxicity amelioration and inhibition effects on p-α-syn accumulation were slightly weaker when GQDs were applied 3 days after α-syn PFF injection, the collective results practically show consistent effects (Supplementary Fig. 8a–f). To verify the cellular localization of the inhibitory effects of GQDs, GQDs, α-syn PFFs and the lysosome were distinctively labelled with fluorescent probes for live imaging (Supplementary Fig. 8g,h). As shown from the time-course snapshots, fluorescence signals for α-syn PFFs and GQDs are co-localized within the lysosome, where the signal for α-syn PFFs gradually decreases and that of GQDs increases with time. It can be presumed that both GQDs and α-syn PFFs are endocytosed, and the disaggregation of fibrillized α-syn takes place in the lysosome by the surrounding GQDs.

One of the key features of the α-syn PFFs neuron model is neuron-to-neuron transmission of pathologic α-syn aggregates[5]. To examine the effect of GQDs, a triple-compartment microfluidic culture device was used, where transmission between neurons takes place sequentially from C1 to C3 (Fig. 3h). At 14 days post-α-syn PFF treatment, the levels of p-α-syn were visualized by immunostaining in all test chambers. The levels of p-α-syn immunoreactivity are greatly reduced in C2 and C3 with the presence of GQDs in C1, which suggests that GQDs prevent the seeds of endogenous α-syn from forming aggregates (Fig. 3i,j). Also, the levels of p-α-syn immunoreactivity are lowered in C2 and C3 when GQDs are added to C2, indicating that GQDs block the transmission of pathologic α-syn to neighbouring neurons.

To address whether GQDs possess neuroprotective effects against α-syn PFF-induced transmission and toxicity in vivo, α-syn PFFs were stereotaxically injected into the striatum of wild-type (WT) mice and GQDs were administered biweekly (that is, every two weeks) via intraperitoneal (i.p.) injection (Fig. 4a). Foremost, we sought to verify the blood–brain barrier (BBB) permeability of GQDs by using an in vitro BBB model[14] (Supplementary Fig. 9a,b). The form and functionality of the BBB model were subsequently confirmed by measuring the transepithelial electrical resistance (TEER) and dextran fluorescence intensity (Supplementary Fig. 9c,d). The in vitro permeability of GQDs was then ascertained by

measuring the fluorescence intensity on the brain side. Intriguingly, the fluorescence signal gradually increased with time, and showed 100% permeability after 24 h (Supplementary Fig. 9e). To corroborate the penetration process visually, GQD–biotin was utilized and linked to streptavidin–quantum dots for live fluorescence imaging. Before the study, the functional behaviour of GQD–biotin was assessed, and was found to exhibit similar BBB penetration rates and fibril dissociation effects as those of pristine GQDs (Supplementary Fig. 9e–g). Live fluorescence imaging showed that the GQD–biotin complex is localized in the lysosome of both brain microvascular endothelial cells (BMECs) and astrocytes, and disappears through the exosome (Supplementary Fig. 9h,i). This suggests that GQDs are endocytosed into BMECs on the blood side and released, then subsequently endocytosed by astrocytes on the brain side and released through the exosome. The in vivo permeability of the BBB was studied by using GQD–biotin for immunohistochemical analysis of the brain. After i.p. injection, a considerable amount of GQD–biotin was detected in the entire central nervous system (CNS) region, including the olfactory bulb, neocortex, midbrain and cerebellum, indicating that GQDs also have the ability to penetrate the BBB in vivo (Supplementary Fig. 9j–n).

At 180 days post-α-syn PFF injection, decreased tyrosine hydroxylase (TH)- and Nissl-positive neurons in the substantia nigra are observed in WT mice. On the other hand, mice administered with GQDs are protected against α-syn PFF-induced loss of dopaminergic neurons (Fig. 4b,c). Furthermore, α-syn PFFs provoke a loss of TH-positive striatal fibre neurons, while GQDs also prevent loss in the striatum (Fig. 4d,e). Finally, changes in the behavioural deficits were assessed by cylinder and pole tests. Mice with GQD injection exhibited alleviated motor deficit, showing balanced use of both forepaws and decreased pole descending time, respectively, in the cylinder and pole tests (Fig. 4f,g).

The levels of p-α-syn, a marker of LBs/LNs, were visualized in the striatum and substantia nigra of α-syn PFF-injected mice. Stereotaxically injected α-syn PFFs provoke accumulation of p-α-syn in the striatum and substantia nigra, but administration of GQDs reduces p-α-syn levels (Fig. 4h,i). The injection of α-syn PFFs in the striatum also leads to propagation of α-syn aggregates throughout the CNS region, whereas GQDs inhibit the transmission of pathological α-syn (Fig. 4j). In addition, GQDs injection ameliorates α-syn PFF-induced gliosis in the substantia nigra accompanying decreased microglia density and glial fibrillary acidic protein (GFAP) levels in astrocytes (Supplementary Fig. 10). To further corroborate the therapeutic potential of GQDs against a transgenic in vivo Parkinson's disease model, 6 month human A53T α-syn transgenic mice[15] were administered biweekly with GQDs for 4 months (Supplementary Fig. 11a). Similar to the α-syn PFF-induced model, GQDs administration reduces p-α-syn levels in the CNS region (Supplementary Fig. 11b–d), as well as the microglia density and GFAP levels in astrocytes in the transgenic model (Supplementary Fig. 11h–k). GQDs treatment also reduces the α-syn aggregates induced by overexpression of human A53T α-syn in HEK293 cells[16] (Supplementary Fig. 11l,m). GQDs alleviate behavioural defects in the hA53T α-syn Tg mice as well, as monitored by the pole and clasping tests (Supplementary Fig. 11e–g). It must be noted that there is no loss of dopamine neurons, glial cells activation, behavioural abnormalities and organ damage in mice with 6 months of prolonged GQDs injection, demonstrating that

GQDs manifest no appreciable long-term in vitro and in vivo toxicity and can be cleared from the body and excreted into urine (Supplementary Fig. 12).

A few previous reports have discussed the potential therapeutic role of graphene oxides (GOs) and GQDs against Alzheimer's disease by inhibiting the fibrillization of beta-amyloid (Aβ) peptides[17–19]. In addition, computational evidence suggests that a hydrophobic graphene sheet could cause the destruction of amyloid fibrils[20]. To compare the therapeutic efficacy of GQDs with the results of previous studies, nanosized GOs (nano-GOs, ranging from ~5 to 20 nm) and reduced GQDs (rGQDs) were prepared (Supplementary Fig. 13a,b). As shown from the Fourier-transform infrared (FT–IR) spectra, pristine GQDs exhibit abundant carboxyl groups, while nano-GOs and rGQDs show much lower carboxyl group:aromatic carbon double bond ratios. The difference in the carboxyl functional group contents is directly reflected in cell viability assays, where nano-GOs and rGQDs show serious in vitro toxicities, unlike GQDs (Supplementary Fig. 13c,d). Moreover, nano-GOs and rGQDs exhibit considerably weaker fibril-dissociation effects than GQDs (Supplementary Fig. 13e–g). This can presumably be attributed to the presence of fewer carboxyl functional groups as well, as we have verified from the ^{1}H–^{15}N HSQC analysis that the positively charged N-terminal region is the initial, but chief binding site with GQDs. It must also be noted that the BBB permeability of nano-GOs is much lower than that of GQDs and rGQDs, suggesting that size may be a decisive factor for the BBB permeability of graphene-based nanoparticles (Supplementary Fig. 13h). Collectively, our results show that GQDs are the optimal therapeutic candidate for anti-Parkinson's disease and related α-synucleinopathies therapy, with no appreciable in vitro and long-term in vivo toxicity, respectable fibril dissociation effects, and the ability to pass through the BBB.

To open new venues in clinical drug development against Parkinson's disease, a candidate desirably features outstanding anti-aggregation and dissociation properties towards α-syn aggregates, without severe toxicity. GQDs are found to bind to α-syn fibrils, inhibit transmission and possess unique neuroprotective effects against the neuropathological α-syn aggregates/fibrils in both in vitro and in vivo models. It is expected that GQD-based drugs with appropriate modifications might provide a clue to support the development of new therapeutic agents for abnormal protein aggregation-related neurological disorders including Parkinson's disease.

Methods

Methods, including statements of data availability and any associated accession codes and references, are available at https://doi.org/10.1038/s41565-018-0179-y.

Methods

Preparation of GQDs.

GQDs were synthesized by placing 0.9 g of carbon fibres (Carbon Make) in a mixture of strong acid (300 ml sulphuric acid and 100 ml nitric acid; Samchun Chemical) at 80 °C for 24 h. After acid removal, the solution was vacuum-filtered with a porous inorganic membrane filter (cat. no. 6809–5002, Whatman-Anodisc 47; GE Healthcare) to discard large

particles. The solution was then subjected to rotary evaporation to yield the final product in powder form.

FT–IR measurements.

The samples were prepared through the conventional KBr pellet method (no. of scans, 32; resolution, 4; wavenumber range, 4,000–40 cm^{-1}). The analysis was performed with a Nicolet 6700 FT–IR spectrometer (Thermo Scientific).

ThT and turbidity assays.

Turbidity and ThT assays were used for the measurement of α-syn fibrils. For the ThT assay, 50 μl of each sample was centrifuged at 16,000g- for 30 min. The pellet was then resuspended in 200 μl of ThT assay solution consisted of 25 μM ThT (cat. no. T3516, Sigma-Aldrich) in 10 mM glycine buffer (pH 9.0). The amount of α-syn fibrils was determined by a fluorescence spectrophotometer with the ThT fluorescence measured at 482 nm (excitation at 440 nm). For the turbidity assay, α-syn fibrils were diluted with PBS (1:10). The diluted α-syn fibrils were loaded into the wells of Corning 96-well plates. The turbidity of each sample was determined by a microplate reader (absorbance at 360 nm).

TEM imaging.

The α-syn fibrils were adsorbed to glow discharge grids (EMS, 400 mesh carbon-coated copper grids) for 2 min and rinsed with three drops of Tris-HCl (50 mM, pH 7.4). The rinsed grids were floated with two drops of 0.75% uranyl formate. After drying, the images were captured by a Phillips CM 120 TEM (80 kV) with an AMT ER–80 ° charge-coupled device (8 megapixel). For primary cultured neurons, cells were seeded onto a poly-D-lysine-coated 35 mm dish at a density of 100,000 cells per well. Neurons were treated with 1 μgml^{-1} of PFFs with or without 1 μgml^{-1} of GQDs at days in vitro (DIV) 10. At DIV 17, cells were washed with 1% sodium nitrite containing PBS (pH 7.4) and fixed with 3% PFA, 100 mM cacodylate, 1.5% glutaraldehyde, 2.5% sucrose containing fixative (pH 7.4) for 1 h. TEM images were captured by a Philips EM 410 TEM with a Soft Imaging System Megaview III digital camera.

Dot-blot assays.

Tris-buffered saline (TBS)-wetted nitrocellulose membrane (NC membrane, 0.45 μm pore) was mounted on the Bio-Dot microfiltration apparatus (cat. no. 1706545, Bio-Rad). The samples were loaded into the wells of a microfiltration apparatus under mild vacuum. After washing with TBS, the NC membranes were blocked with 0.5% Tween-20 and 5% non-fat dry milk containing TBS blocking buffer and attached with anti-α-syn filament antibody (cat. no. ab209538, 1:1,000, abcam) at 4 °C for 12 h. After incubation with horseradish peroxidase (HRP)-conjugated rabbit second antibodies (GE Healthcare) at room temperature for 1 h, the signals from α-syn aggregates were then visualized by enhanced chemiluminescence (ECL) solution. The data were analysed with ImageJ software (http://rsb.info.nih.gov/ij/, NIH).

BN–PAGE and SDS–PAGE.

For BN–PAGE, α-syn fibrils and α-syn PFFs were prepared using a NativePAGE sample prep kit (cat. no. BN2008, Life Technologies) and run on NativePAGE Novex 4–16% bis–tris protein gels (cat. no. BN1002Box, Life Technologies) at 200 V for 90 min. Then, 50 mM tricine, 15 mM Bis–Tris, 0.02% Brilliant Blue G (pH 7.0) containing cathode buffer and 50 mM Bis–Tris (pH 7.0) containing anode buffer were used for BN–PAGE. After BN–PAGE, gels were stained with a SilverQuest silver staining kit (cat. no. LC6070, Life Technologies), following the manufacturer's protocols. For SDS–PAGE, 10 DIV cortical neurons were treated with α-syn PFFs (5 µgml^{-1}) in the presence and absence of GQDs (5 µgml^{-1}) for 7 days. At DIV 17, the soluble proteins were isolated from the neurons with a 1% TX-100, protease inhibitors and phosphatase inhibitors cocktail (cat. no. PPC1010, Sigma-Aldrich) containing sample buffer. For insoluble protein isolation, the lysates of neurons were sonicated and centrifuged at 12,000g for 30 min at 4 °C. The remaining pellet was washed and suspended in 2% SDS containing PBS for preparation of insoluble protein. Laemmli sample buffer (2×, cat. no. 1610737, Bio-Rad) was used to dilute the soluble and insoluble protein samples. For SDS–PAGE, 20 µg of soluble or insoluble proteins was loaded onto the wells of Novex 8–16% tris-glycine gel (cat. no. XP08160B0X, Life Technologies) and electrophoresis was performed at 130 V for 85 min. After transfer of proteins onto the NC membrane, it was blocked with 0.1% Tween-20 and 5% non-fat dry milk containing TBS for 1 h and incubated at 4 °C overnight with SNAP25 (cat. no. 111–002, 1:2,000, Synaptic Systems), VAMP2 (cat. no. ab3347, 1:1,000, abcam) or anti-pS129-α-syn antibodies (cat. no. ab59264, 1:1,000, abcam). The NC membranes were then incubated with HRP-conjugated mouse or rabbit secondary antibodies (GE Healthcare) at room temperature for 1 h and visualized by ECL solution. The signals were measured by ImageJ software (http://rsb.info.nih.gov/ij/, NIH).

Preparation of sonicated α-syn PFFs.

The α-syn PFFs were prepared following the method published in ref.[21]. Briefly, full-length mouse recombinant α-syn was cloned using the pRK172 bacterial expression vector. The plasmids were then transformed into BL21(DE3)RIL-competent *Escherichia coli* (cat. no. 230245, Life Technologies). The α-syn monomers were purified through several steps including dialysis, anion exchange and size exclusion chromatography after bacterial growth. In vitro α-syn fibrils were assembled in an Eppendorf orbital mixer (cat. no. 538400020) under specific agitation conditions (1,000 r.p.m., 37 °C, 7 days). For the formation of preformed fibrils, α-syn fibrils were sonicated for a total of 60 pulses (20% amplitude, 0.5 s on, 0.5 s off) with a 1/8″ probe sonicator.

Biotinylation of GQDs and binding assay.

GQDs (50 mg) were dissolved in conjugation buffer (pH 4.7), and 12.5 mg of EDC reagent (*N*-(3-dimethylaminopropyl)-*N*″-ethylcarbodiimide hydrochloride; cat. no. 03449, Sigma-Aldrich) was subsequently added to replace the carboxyl groups. After 1 h of reaction with vigorous stirring, 25 mg of EZ-Link amine-PEG$_3$-biotin (cat. no. 21347; Thermo Scientific) was added to EDC-activated GQDs. The solution was then subjected to dialysis and rotary evaporation to yield the final product in powder form. For the binding assay between GQDs

and α-syn fibrils, 5 mg ml^{-1} of α-syn fibrils were incubated with 5 mg ml^{-1} of biotinylated GQDs and streptavidin-conjugated 0.8 nm ultra-small gold particles (cat. no. 800.099, Aurion) for 1 h. Next, the streptavidin-conjugated ultra-small gold particles bound with high affinity to biotinylated-GQDs were enhanced with GoldEnhance EM Plus solution (cat.no. 2114, Nanoprobes) for 5 min. Non-reacted solution was removed by a 100 kDa molecular weight cut-off spin column (cat. no. UFC510024, Millipore-Sigma), followed by TEM analysis.

Purification of ^{15}N-labelled α-syn.

The α-syn gene cloned in pRK172 vector was transformed into *E. coli* BL21 (DE3) for α-syn overexpression. For the preparation of isotope-labelled α-syn, cells were grown in M9 minimal medium containing 0.5 g of ^{15}NH$_4$Cl and 1 g of ^{13}C glucose (Cambridge Isotope Laboratory) per litre at 37 °C with 100 μgml^{-1} ampicillin. After induction with isopropyl β-D-1-thiogalactopyranoside (IPTG), the heat-treated cell lysate was subjected to successive purifications using DEAE-Sephacel anion-exchange, Sephacryl S-200 size-exclusion and S-Sepharose cation-exchange chromatography. The purified α-syn was dialysed against 12 l of fresh 20 mM 2-(*N*-morpholino)ethanesulfonic acid (MES) buffer (pH 6.5) three times, and stored in aliquots at a concentration of 1 mg ml^{-1} at –80 °C. The sample was concentrated to 5 mg ml^{-1} using Nanosep 10K membrane (Pall Gelman) at 4 °C immediately before the experiments.

NMR spectroscopy analysis.

A detailed NMR study of the interaction between α-syn and GQDs was performed using a 950 MHz spectrometer equipped with a cryo-genic probe (Bruker). ^{15}N-labelled α-syn (5 mg ml^{-1}, 100 μl) was reacted with GQDs (5 mg ml^{-1}, 100 μl) under 37 °C shaking incubation at 1,000 r.p.m. for 3 days. ^{15}N-labelled α-syn samples were prepared using 20 mM MES buffer (pH 6.5) containing 10% for ^{1}H–^{15}N HSQC measurements. ^{1}H–^{15}N HSQC spectra of both α-syn and GQD-reacted α-syn were acquired at 37 °C. The obtained data were processed by NMRPipe[22] and analysed by Sparky[23].

Simulation details.

The MS simulation (200 ns) was performed with Gromacs 5.1 to examine the interaction between GQDs and α-syn fibrils at the molecular level[24]. The initial structure of the hydrophobic NAC domain (residues 71–82) of α-syn was adapted from the ssNMR structure (PDB ID: 2N0A) with CHARMM forcefield[25], and the structure of the GQDs was designed with CGenFF[26] by protocols from https://cgenff.paramchem.org.

CD measurements.

The α-syn fibrils (5 mg ml^{-1}, 100 μl) were mixed with GQDs solution (5 mg ml^{-1}, 100 μl) and depolymerized under 37 °C shaking incubation at 1,000 r.p.m. for 7 days. For far-ultraviolet CD measurements, the sample was diluted (1/2) with deionized water. CD spectra between 190 and 260 nm were measured at 0.5 nm intervals using a J-815 spectropolarimeter (Jasco) and a 0.2-mm-path-length quartz cuvette. The spectrum of the buffer solution was subtracted from the sample spectra. CD signals were normalized to the

mean residue ellipticity, [θ], with units of deg cm2 dmol^{-1}. The fractional secondary structure contents of the α-syn fibrils and depolymerized α-syn fibrils were calculated using the algorithm of CONTIN/LL on the DichroWeb online server (http://dichroweb.cryst.bbk.ac.uk). For the calculation using CONTIN/LL, reference set 7 on Dichroweb was employed, which is optimized for the wavelength range 190–240 nm.

Primary neuron culture.

Primary cortical neurons were isolated from the brain of embryonic day 15 C57BL/6 mice (Charles River) and seeded onto poly-D-lysine-coated dishes (cat. no. P6407, Sigma-Aldrich). The cultured neurons were maintained with complete culture medium composed of B27 supplement (cat. no. 17504044, Life Technologies), L-glutamine (cat. no. 25030149, Life Technologies) and neurobasal medium (cat. no. 21103049, Life Technologies) at 37 °C in a 7% CO_2 incubator. To inhibit the growth of glial cells in the neuron culture, 30 μM of 5-fluoro-2′-deoxyuridine (cat. no. F0503, Sigma-Aldrich) was added after 5 days of culture.

Cell viability and cytotoxicity assays.

For cell viability and cytotoxicity assays, primary cortical neurons were seeded onto poly-D-lysine-coated glass coverslips at a density of 10,000 cells per cm^2. The cells were then incubated in a 7% CO_2 incubator at 37 °C with complete neuronal culture medium. The cytotoxicity was measured with α-syn PFFs (1 μgml^{-1}) in the absence and presence of GQDs (1 μgml^{-1}) in 10 DIV primary mouse cortical neurons for 7 days. An LDH cytotoxicity assay kit (cat. no. 88954, Pierce) and TUNEL assay kit (cat. no. 12156792910, Roche) were used to measure cytotoxicity. The viability of mouse primary cortical neurons and SH-SY5Y cells was determined using an alamarBlue cell viability assay kit (cat. no. DAL1025, Molecular Probes) and a neurite outgrowth staining kit (cat. no. A15001, Molecular Probes), following the manufacturers' instructions.

In vitro immunofluorescence.

Mouse primary cortical neurons were seeded at a density of 20,000 cells per cm^2 onto poly-D-lysine-coated glass coverslips. After the cells were fixed with 4% PFA and blocked with 5% normal donkey serum (NDS; cat. no. 017-000-121, Jackson ImmunoResearch), 2% bovine serum albumin (BSA; cat. no. A7030, Sigma-Aldrich) and 0.1% Triton X-100 (cat. no. T8787, Sigma-Aldrich) containing PBS at room temperature for 1 h. Subsequent incubations with anti-8-OHG (cat. no. ab62623, 1:1,000, abcam), anti-pS129-α-syn (cat. no. ab59264, 1:1,000, abcam) and anti-MAP2 (cat. no. MAB3418, 1:1,000, Millipore) antibodies were carried out overnight at 4 °C. The coverslips were washed with 0.1% Triton X-100 containing PBS and incubated with a mixture of FITC-conjugated (donkey anti-rabbit FITC, cat. no. 711-095-152; donkey anti-mouse FITC, cat. no. 715-095-151, Jackson ImmunoResearch) and Cy3-conjugated (donkey anti-rabbit CY3, cat. no. 711-165-152; donkey anti-mouse CY3, cat. no. 715-165-151, Jackson ImmunoResearch) second antibodies at room temperature for 1 h. The fluorescence images were captured using a Zeiss LSM 710 confocal microscope.

Microfluidic chambers.

Before being fixed to the microfluidic devices (triple-chamber microfluidic devices, cat. no. TCND1000, Xona), the rectangular glass coverslips were prepared according to the method of ref.[5]. Each chamber was plated at a density of 100,000 cells per chamber. At DIV 7, 0.5 μg of GQDs were added to chamber 1 (C1) or chamber 2 (C2) before treatment with 0.5 μg α-syn PFFs to C1. To regulate the direction of flow of the channels, a 50 μl difference in media volume was controlled through the chambers. At DIV 21, neurons in the chambers were fixed with 4% PFA containing PBS and blocked with 0.1% Triton X-100, 5% NDS and 2% BSA containing PBS at room temperature for 1 h. The chambers were then incubated with anti-pS129-α-syn (cat. no. ab59264, 1:1,000, abcam) and anti-MAP2 (cat. no. MAB3418, 1:1,000, Millipore) antibodies at 4 °C, overnight. After washing the chambers with 0.1% Triton X-100 containing PBS, the chambers were incubated in a mixture of FITC-conjugated (Jackson ImmunoResearch) and Cy3-conjugated (Jackson ImmunoResearch) second antibodies for 1 h at room temperature. The fluorescent images were captured using a LSM 710 Zeiss confocal microscope.

Animals.

All animal-based experimental procedures followed the guidelines of the Laboratory Animal Manual of the NIH Guide to the Care and Use of Animals. The procedures were approved by the Animal Care and Use Committee of Johns Hopkins Medical Institute. The human α-syn-A53T transgenic mice (stock no. 006823, B6.Cg-Tg, Prnp-SNCA*A53T;23Mkle/J) were purchased from the Jackson Laboratory[27].

Stereological assessments.

C57BL/6 mice (8- to 10-week-old males) for stereological injection were purchased from the Jackson Laboratory. After anaesthetizing with 60 mg kg^{-1} of pentobarbital sodium solution, mice were injected with PBS (2 μl) or PFFs (5 μg per 2 μl) by stereotaxic instruments (cat. no. Model 900, David KOPF instruments). The designated coordinate of the injection site of the striatum was +2.0 mm from the midline, +2.6 mm beneath the dura, and + 0.2 mm relative to the bregma. As a treatment, 50 μl of GQDs (50 μg per mouse) were i.p. injected for 6 months on a biweekly (every two weeks) basis. After 6 months of GQDs injection, mice were perfused and fixed with 4% PFA containing PBS for 12 h, followed by cryoprotection with 30% sucrose. For TH and Nissl staining, 50 μm coronal sections were cut using a cryostat (Bio-Rad), and every fourth section was used for stereological assessment. Sections were incubated with rabbit polyclonal anti-TH (cat. no. NB300–19, 1:1,000, Novus Biologicals) or rabbit polyclonal anti-pS129-α-syn (cat. no. ab59264, 1:1,000, abcam) with 5% NDS, 0.1% TX-100 containing PBS blocking solution. The sections were then incubated with streptavidin-conjugated HRP and biotinylated secondary antibodies (cat. no. PK-6101, Vector Laboratories). Immune-positive signals were visualized using a DAB kit (cat. no. SK-4100, Vector Laboratories). To identify the Nissl substance, the TH-stained tissues were counterstained with thionin-containing staining solution. The total number of TH- and Nissl-positive neurons in the SN region was quantified by microscopy with Stereo Investigator software (MBF Bioscience).

In vivo immunohistochemistry.

The isolated brains were perfused and fixed with 4% PFA containing PBS. After cryoprotection with 30% sucrose, mouse brain sections were incubated with anti-GFAP (cat. no. Z0334, 1:2,000, Dako) or anti-Iba-1 (cat. no. 019–19741, 1:1,000, Wako) antibodies with blocking solution. The brain sections were then followed by incubation with biotin-tagged anti-rabbit second antibody. After incubation with ABC solution (cat. no. PK-6101, Vector Laboratories), brain sections were developed using a DAB peroxidase substrate kit (cat. no. SK-4100, Vector Laboratories). The densities of astrocytes and total number of microglia were measured in the substantia nigra region by ImageJ software (http://rsb.info.nih.gov/ij/, NIH). For histopathology of major organs such as the liver, kidney and spleen, 8- to 10-week-old male C57BL/6 mice were i.p. injected with 50 µg of GQDs on a biweekly basis for 6 months. After the 6 months of injections, mice were perfused with 4% PFA containing PBS. The liver, kidney and spleen were then stained with an H&E staining kit (cat. no. H-3502, Vector Laboratories).

Behaviour analyses.

The cylinder test[28] was devised to identify any asymmetry in forelimb use. Every contact made by a forepaw in a 20-cm-wide clear glass cylinder was scored by a blinded observer using video clips. No habituation of the mice to the testing cylinder was allowed before making the video clips. A total of 20 to 30 wall touches were counted per animal (only contacts with fully extended forelimbs). The degree of impaired forelimb touches was converted to percentage based on the total forelimb use. The control group scored approximately 50% in this test. The mice were completely isolated from the test cylinder before actual testing.

For the pole test[29], test mice were allowed to adapt to the behavioural room for 30 min before testing. A 75 cm metal pole with a diameter of 9 mm was prepared with bandage gauze wrapping. To initiate the test, each mouse was placed 7.5 cm from the top facing upwards. The scores were based on the total time taken to reach the bottom. The test animals were trained for two successive days before the actual trial, where each practice provided three different trials. No more than 60 s was allowed for each animal. The results for the turn down, climb down and the total time (in seconds) were recorded.

Statistics.

Mean ± s.d. values were determined from more than three independent experiments. To determine the statistical significance, P values were determined by Student's t-test or ANOVA with Bonferroni correction. Prism6 software was used for statistics analysis.

Reporting Summary.

Further information on experimental design is available in the Nature Research Reporting Summary linked to this article.

Data availability.

There are no data relevant to accession codes or unique identifiers non-publicly available. The data that support the plots within this paper and other findings of this study are available from the corresponding authors upon reasonable request.

Supplementary Material

Refer to Web version on PubMed Central for supplementary material.

Acknowledgements

References

1. Dawson TM & Dawson VL Molecular pathways of neurodegeneration in Parkinson's disease. Science 302, 819–822 (2003). [PubMed: 14593166]

2. Spillantini MG et al. Alpha-synuclein in Lewy bodies. Nature 388, 839–840 (1997). [PubMed: 9278044]

3. Li JY et al. Lewy bodies in grafted neurons in subjects with Parkinson's disease suggest host-to-graft disease propagation. Nat. Med 14, 501–503 (2008). [PubMed: 18391963]

4. Desplats P et al. Inclusion formation and neuronal cell death through neuron-to-neuron transmission of alpha-synuclein. Proc. Natl Acad. Sci. USA 106, 13010–13015 (2009). [PubMed: 19651612]

5. Volpicelli-Daley LA et al. Exogenous alpha-synuclein fibrils induce Lewy body pathology leading to synaptic dysfunction and neuron death. Neuron 72, 57–71 (2011). [PubMed: 21982369]

6. Luk KC et al. Pathological alpha-synuclein transmission initiates Parkinson-like neurodegeneration in nontransgenic mice. Science 338, 949–953 (2012). [PubMed: 23161999]

7. Varela L, Bell CH, Armitage JP & Redfield C 1H, 13C and ^{15}N resonance assignments for the response regulator CheY3 from *Rhodobacter sphaeroides*. Biomol. NMR Assign. 10, 373–378 (2016). [PubMed: 27468962]

8. Bodner CR, Dobson CM & Bax A Multiple tight phospholipid-binding modes of alpha-synuclein revealed by solution NMR spectroscopy. J. Mol. Biol 390, 775–790 (2009). [PubMed: 19481095]

9. Tuttle MD et al. Solid-state NMR structure of a pathogenic fibril of full-length human alpha-synuclein. Nat. Struct. Mol. Biol 23, 409–415 (2016). [PubMed: 27018801]

10. Giasson BI, Murray IVJ, Trojanowski JQ & Lee VMY A hydrophobic stretch of 12 amino acid residues in the middle of alpha-synuclein is essential for filament assembly. J. Biol. Chem 276, 2380–2386 (2001). [PubMed: 11060312]

11. van Stokkum IH, Spoelder HJ, Bloemendal M, van Grondelle R & Groen FC Estimation of protein secondary structure and error analysis from circular dichroism spectra. Anal. Biochem 191, 110–118 (1990). [PubMed: 2077933]

12. Sreerama N & Woody RW Estimation of protein secondary structure from circular dichroism spectra: comparison of CONTIN, SELCON, and CDSSTR methods with an expanded reference set. Anal. Biochem 287, 252–260 (2000). [PubMed: 11112271]

13. Lin MT & Beal MF Mitochondrial dysfunction and oxidative stress in neurodegenerative diseases. Nature 443, 787–795 (2006). [PubMed: 17051205]

14. Czupalla CJ, Liebner S & Devraj K In vitro models of the blood–brain barrier. Methods Mol. Biol 1135, 415–437 (2014). [PubMed: 24510883]

15. Lee MK et al. Human α-synuclein-harboring familial Parkinson's disease-linked Ala-53→Thr mutation causes neurodegenerative disease with α-synuclein aggregation in transgenic mice. Proc. Natl Acad. Sci. USA 99, 8968–8973 (2002). [PubMed: 12084935]

16. Brahmachari S et al. Activation of tyrosine kinase c-Abl contributes to α-synuclein-induced neurodegeneration. J. Clin. Invest 126, 2970–2988 (2016). [PubMed: 27348587]

17. Li Q et al. Modulating Aβ$_{33-42}$ peptide assembly by graphene oxide. Chem. Eur. J 20, 7236–7240 (2014). [PubMed: 24838837]

18. Mahmoudi M, Akhavan O, Ghavami M, Rezaee F & Ghiasi SMA Graphene oxide strongly inhibits amyloid beta fibrillation. Nanoscale 4, 7322–7325 (2012). [PubMed: 23079862]

19. Liu Y et al. Graphene quantum dots for the inhibition of beta amyloid aggregation. Nanoscale 7, 19060–19065 (2015). [PubMed: 26515666]

20. Yang ZX et al. Destruction of amyloid fibrils by graphene through penetration and extraction of peptides. Nanoscale 7, 18725–18737 (2015). [PubMed: 26503908]

21. Volpicelli-Daley LA, Luk KC & Lee VM Addition of exogenous alpha-synuclein preformed fibrils to primary neuronal cultures to seed recruitment of endogenous alpha-synuclein to Lewy body and Lewy neurite-like aggregates. Nat. Protoc 9, 2135–2146 (2014). [PubMed: 25122523]

22. Delaglio F et al. NMRPipe: a multidimensional spectral processing system based on UNIX pipes. J. Biomol. NMR 6, 277–293 (1995). [PubMed: 8520220]

23. Lee W, Tonelli M & Markley JL NMRFAM-SPARKY: enhanced software for biomolecular NMR spectroscopy. Bioinformatics 31, 1325–1327 (2015). [PubMed: 25505092]

24. Abraham MJ et al. GROMACS: High performance molecular simulations through multi-level parallelism from laptops to supercomputers. SoftwareX 1–2, 19–25 (2015).

25. Mackerell AD, Jr., Feig M & Brooks CL, III Extending the treatment of backbone energetics in protein force fields: limitations of gas-phase quantum mechanics in reproducing protein conformational distributions in molecular dynamics simulations. J. Comput. Chem 25, 1400–1415 (2004). [PubMed: 15185334]

26. Yu W, He X, Vanommeslaeghe K & MacKerell AD, Jr. Extension of the CHARMM General Force Field to sulfonyl-containing compounds and its utility in biomolecular simulations. J. Comput. Chem 33, 2451–2468 (2012). [PubMed: 22821581]

27. Lee MK et al. Human α-synuclein-harboring familial Parkinson's disease-linked Ala-53→Thr mutation causes neurodegenerative disease with α-synuclein aggregation in transgenic mice. Proc. Natl Acad. Sci. USA 99, 8968–8973 (2002). [PubMed: 12084935]

28. Peelaerts W et al. α-Synuclein strains cause distinct synucleinopathies after local and systemic administration. Nature 522, 340–344 (2015). [PubMed: 26061766]

29. Mao X et al. Pathological α-synuclein transmission initiated by binding lymphocyte-activation gene 3. Science 353, aah3374 (2016). [PubMed: 27708076]
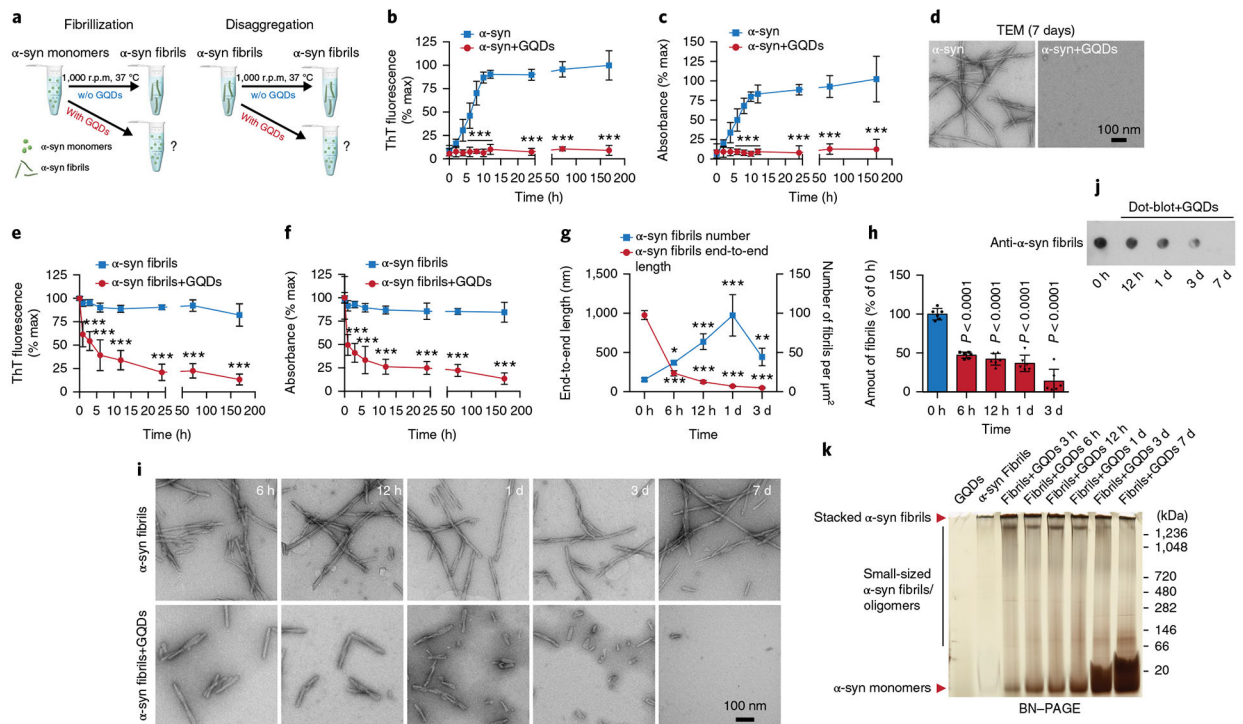
Fig. 1 |. Effect of GQDs on α-syn fibrillization and fibril disaggregation.
a, Schematic representation of α-syn fibrillization (5 mg ml^{-1} α-syn monomers) and disaggregation (5 mgml^{-1} α-syn fibrils) in the presence and absence of GQDs (5 mg ml^{-1}).
b,c, Kinetics of α-syn fibrillization using aliquots of the reaction monitored by ThT fluorescence (**b**) and turbidity assays (**c**) ($n = 4$ biologically independent samples; two-way analysis of variance (ANOVA) with a post hoc Bonferroni test, ***P<0.001; error bars are standard deviation, s.d.). Mean values and P values are provided in Supplementary Table 1.
d, TEM images of α-syn after fibrillization in the absence (left) and presence (right) of GQDs. **e,f**, Kinetics of preformed α-syn fibrils after incubation with GQDs using aliquots of the reaction monitored by ThT fluorescence (**e**) and turbidity assays at various time points (**f**) ($n = 4$ biologically independent samples; two-way ANOVA with a post hoc Bonferroni test, ***P<0.001; error bars are s.d.). Mean values and P values are provided in Supplementary Table 1. **g**, Quantifications of the end-to-end length and number of α-syn fibrils per µm2. Mean values of end-to-end length are 937.84, 245.52, 123.13, 66.27 and 51.02 nm at 0, 6, 12, 24 and 72 h ($n = 50$ fibrils at each time point; one-way ANOVA with a post hoc Bonferroni test, P< 0.0001 at 6, 12, 24 and 72 h; error bars are s.d.). Mean values of number are 15.53, 37.01, 63.83, 97.52 and 44.38 per µm^2 at 0, 6, 12, 24 and 72 h ($n = 6$, biologically independent samples; one-way ANOVA with a post hoc Bonferroni test, $P =$ 0.0483, P<0.0001, P<0.0001 and $P =$ 0.0050 at 6, 12, 24 and 72 h, respectively; error bars are s.d.). **h**, Amount of remaining α-syn fibrils (as % of number at 0 h), determined by multiplying the end-to-end length and number of α-syn fibrils at the same time points (0, 6, 12, 24 and 72 h) in the presence of GQDs. Mean values are 100.00, 47.33, 42.00, 36.67 and 13.83 at 0, 6, 12, 24 and 72 h ($n = 6$, biologically independent samples; one-way ANOVA with a post hoc Bonferroni test, error bars are s.d.). **i**, TEM images of preformed α-syn fibrils at various time points (6 and 12 h, 1, 3 and 7 days) in the absence (top) and presence

(bottom) of GQDs. **j**, Representative image of α-syn fibrils dot-blot assay at various time points (0 and 12 h, 1, 3 and 7days) with α-syn filament specific antibody. These experiments were independently repeated three times with similar results. **k**, BN–PAGE analysis of α-syn, prepared with aliquots of reaction run at various time points (0, 3, 6 and 12 h, 1, 3 and 7days). These experiments were independently repeated three times with similar results.
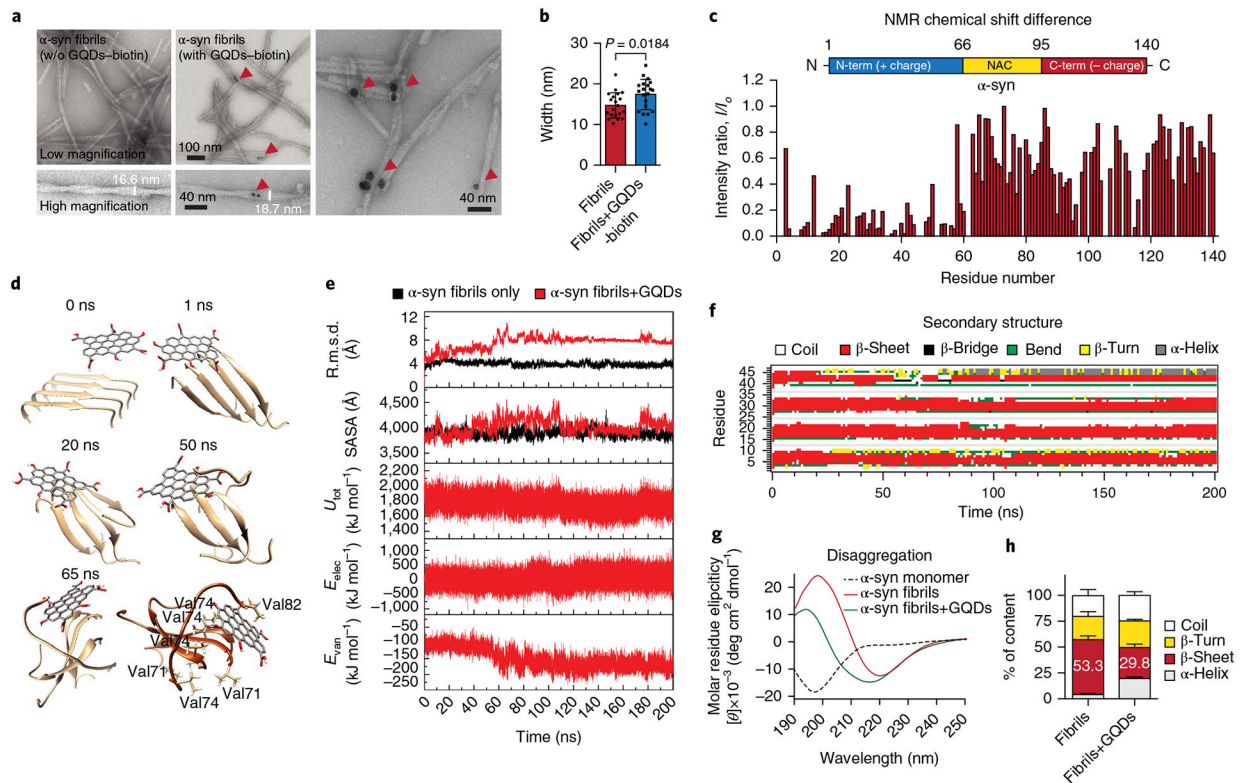
Fig. 2 |. Detailed analysis of the interaction between GQDs and mature α-syn fibrils during the dissociation process.
a, TEM images for binding between biotinylated GQDs and α-syn fibrils with low and high magnifications. Arrowheads indicate biotinylated GQDs enhanced with ultra-small gold-streptavidin nanoparticles. **b**, Quantification of the average width of α-syn fibrils during the disaggregation process after 1 h of incubation (mean±s.d.): 14.74±0.70 nm and 17.42± 0.83 nm for fibrils and fibrils + GQDs-biotin ($n = 20$ for each group, two-tailed Student's t-test). **c**, NMR chemical shift difference obtained from full ^{1}H–^{15}N HSQC spectra. The decreased intensity ratio of NMR chemical shifts is presented for each residue after binding with GQDs. **d**, Time course simulation dynamics of the interaction between GQDs and mature α-syn fibrils, and 65 ns snapshot image (bottom right) of the interaction between GQDs and mature α-syn fibrils with designated sidechains attributed for the major binding force. **e**, Time-dependent plots for r.m.s.d. of atomic positions, SASA for the α-syn fibril only group and α-syn fibril and GQDs group, total potential energy (U_{tot}), electrostatic energy (E_{elec}) and van der Waals energy (E_{van}) for α-syn fibril and GQDs group, respectively (from the top). **f**, Time-dependent secondary structure plot calculated by the DSSP algorithm. **g**, CD spectra of α-syn monomers and α-syn fibrils without and with GQDs after 7 days of incubation. **h**, Fractional secondary structure contents ratio of α-syn fibrils and α-syn fibrils disaggregated by GQDs calculated using the algorithm CONTIN/LL ($n = 5$ biologically independent samples). Data presented as mean± s.d. (fibrils versus fibrils + GQDs (% of content); coil: 20.13± 5.74 versus 24.58±3.64; β-turn: 22.39± 4.62 versus 25.89±1.34; β-sheet: 53.30± 3.53 versus 29.76±3.35; α-helix: 4.17± 1.25 versus 19.74± 1.52).
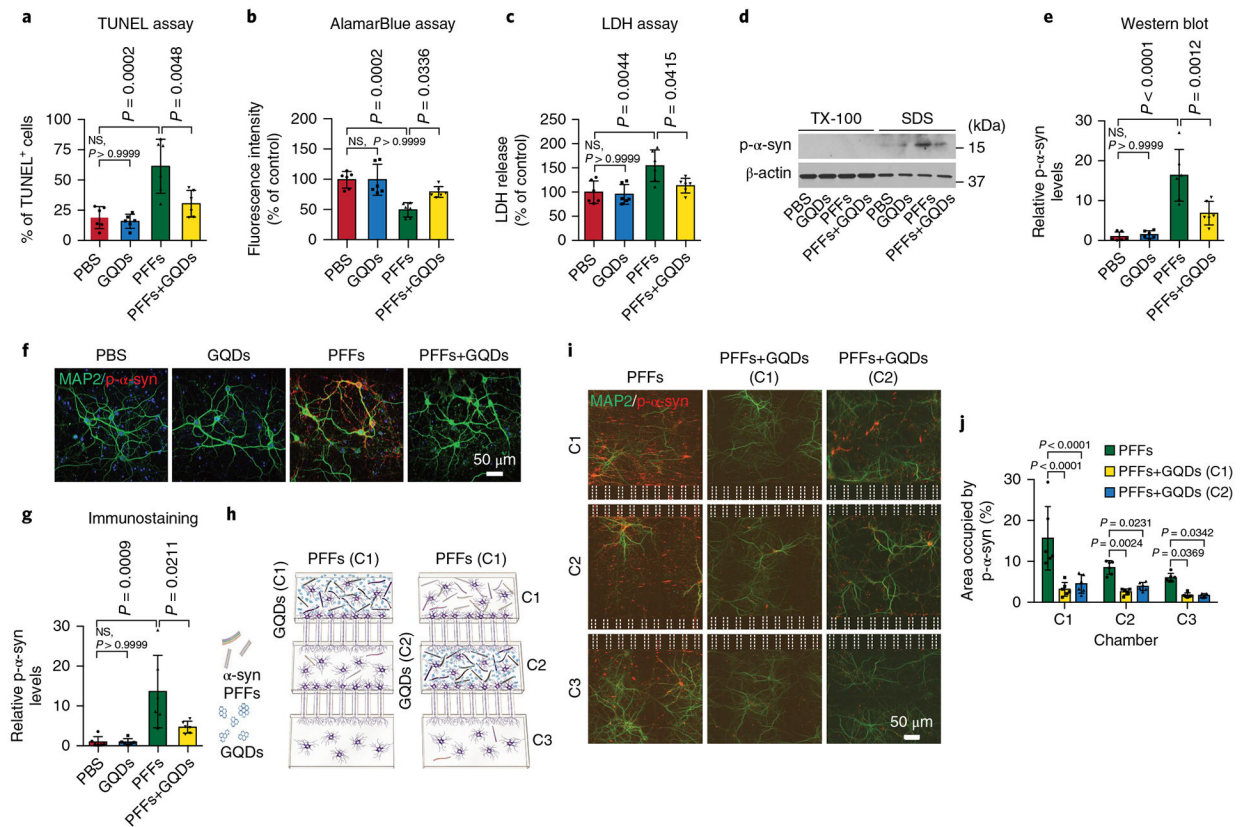
Fig. 3 |. Effect of GQDs on α-syn PFF-induced neuronal death, pathology and transmission in vitro.

a–c, Neuronal death assessed by TUNEL (**a**), alamarBlue (**b**) and LDH assays (**c**) treated with α-syn PFFs (1 μg ml^{-1}) in the absence and presence of GQDs (1 μg ml^{-1}) in 10 DIV mouse cortical neurons for 7 days. Mean values of TUNEL (% of TUNEL+ cells) are 18.94, 15.86, 61.39 and 30.45 for PBS, GQDs, PFFs and PFFs + GQDs; mean values of alamarBlue (% of control) are 100.00, 99.16, 49.33 and 78.86 for PBS, GQDs, PFFs and PFFs + GQDs; mean values of LDH assay (% of control) are 100.00, 95.43, 154.58 and 113.33 for PBS, GQDs, PFFs and PFFs + GQDs ($n = 6$ biologically independent samples; two-way ANOVA with post hoc Bonferroni test; NS, not significant; error bars are s.d.). **d**, Representative immunoblot levels with p-α-syn antibody. **e**, Quantifications of the SDS-insoluble fraction normalized to the levels of β-actin. Mean values are 1.00, 1.49, 16.35 and 6.86 for PBS, GQDs, PFFs and PFFs + GQDs ($n = 6$ biologically independent samples; two-way ANOVA with post hoc Bonferroni test; NS, not significant; error bars are s.d.). **f**, Representative p-α-syn immunostaining micrographs with p-α-syn antibody. **g**, Quantifications of p-α-syn immunofluorescence intensities normalized to PBS control. Mean values are 1.00, 0.99, 13.62 and 4.69 for PBS, GQDs, PFFs and PFFs + GQDs ($n = 6$ biologically independent samples; two-way ANOVA with post hoc Bonferroni test; NS, not significant; error bars are s.d.). **h**, Schematic representation of the microfluidic device for the transmission of pathologic α-syn, composed of three connected chambers. **i**, Representative images of p-α-syn immunostained neurons in the microfluidic device 14days post α-syn PFFs addition. **j**, Quantifications of p-α-syn immunofluorescence intensities. Areas

occupied by p-α-syn were measured in each chamber. Mean values of chamber 1 are 15.67, 3.12 and 4.52 for PFFs, PFFs + GQDs (C1) and PFFs + GQDs (C2); mean values of chamber 2 are 8.52, 2.56 and 3.90 for PFFs, PFFs + GQDs (C1) and PFFs + GQDs (C2); mean values of chamber 3 are 6.04, 1.72 and 1.67 for PFFs, PFFs + GQDs (C1) and PFFs + GQDs (C2) ($n = 6$ biologically independent samples; two-way ANOVA with post hoc Bonferroni test; NS, not significant; error bars are s.d.).
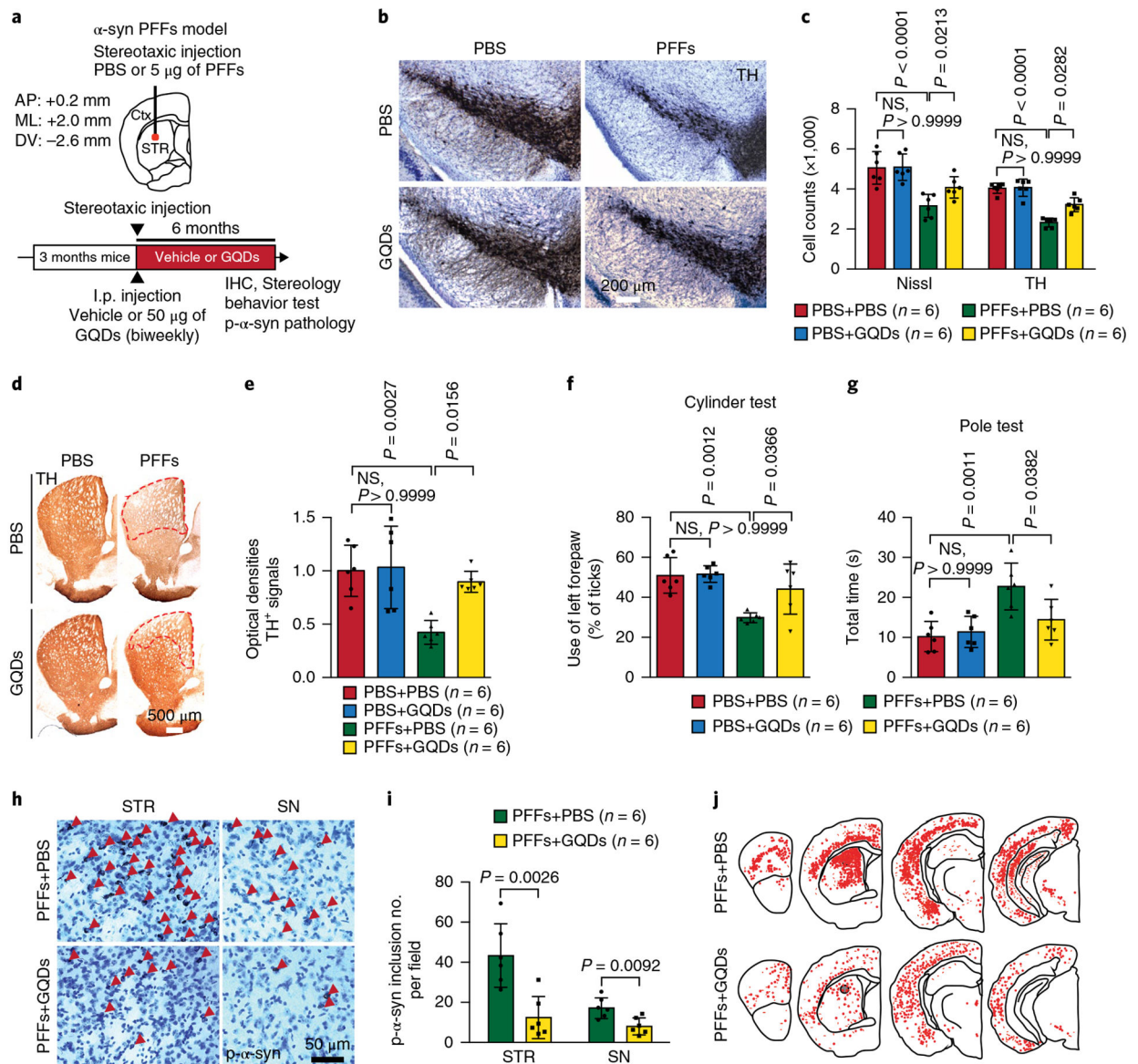
Fig. 4 |. Effect of GQDs on α-syn-induced pathologies in vivo.
a, Schematic illustration of injection coordinates of α-syn PFFs (5μg) for stereotaxic intrastriatal injection in C57BL/6 mice. As a treatment, 50 μg of GQDs or PBS were i.p. injected biweekly for 6 months. AP, anteroposterior; ML, mediolateral; DV, dorsoventral; Ctx, cortex; STR, striatum; IHC, immunohistochemistry. **b**, Representative TH immunohistochemistry images in the substantia nigra of α-syn PFF-injected hemisphere in the absence (top) and presence (bottom) of GQDs. **c**, Stereological counting of the number of TH- and Nissl-positive neurons in the substantia nigra via unbiased stereological analysis after 6 months of α-syn PFF injection with and without GQDs injection. Mean values are 5,061, 5,096, 3,155 and 4,080 Nissl-positive neurons; 4,039, 4,068, 2,327 and 3,221 TH-positive neurons (*n* = 6 biologically independent animals; two-way ANOVA with a post hoc Bonferroni test; NS, not significant; error bars are s.d.). **d**, Representative TH immunohistochemistry images in the striatum of α-syn PFF-injected hemisphere. **e**,

Quantifications of TH-immunopositive fibre densities in the striatum. Mean values for relative optical densities of TH+ signals are 1.00, 1.03, 0.42 and 0.90 for PBS + PBS, PBS + GQDs, PFFs+ PBS and PFFs + GQDs (n = 6 biologically independent animals; two-way ANOVA with a post hoc Bonferroni test; NS, not significant; error bars are s.d.). **f**, Assessments of the behavioural deficits measured by the use of forepaws in the cylinder test. Mean values (% of ticks) are 51.00, 51.67, 29.83 and 44.17 for PBS+ PBS, PBS + GQDs, PFFs + PBS, and PFFs + GQDs (n = 6 biologically independent animals; two-way ANOVA with a post hoc Bonferroni test; NS, not significant; error bars are s.d.). **g**, Assessments of the behavioural deficits measured by the ability to grasp and descend from a pole. Mean values are 10.25, 11.38, 22.73 and 14.43 s for PBS + PBS, PBS + GQDs, PFFs + PBS and PFFs + GQDs (n = 6 biologically independent animals; two-way ANOVA with a post hoc Bonferroni test; NS, not significant; error bars are s.d.). **h**, Representative p-α-syn immunostaining images in the striatum (STR) and substantia nigra (SN) of α-syn PFF-injected hemisphere. **i**, Quantifications of p-α-syn immunoreactive neurons in the striatum and substantia nigra. Mean values (number of inclusions) are 43.33 and 12.50 for PFFs+ PBS and PFFs + GQDs of striatum (STR); 17.67 and 8.00 for PFFs+ PBS and PFFs + GQDs of substantia nigra (n = 6 biologically independent animals; two-tailed Student's t-test; error bars are s.d.). **j**, Distribution of LB/LN-like pathology in the CNS of α-syn PFF-injected hemisphere (p-α-syn positive neurons, red dots; p-α-syn positive neurites, red lines).